Triphenylphosphine-Stabilized Diphenyl-Arsenium, -Stibenium, and -Bismuthenium Salts

Nathan L. Kilah,[†] Simon Petrie,[‡] Robert Stranger,*[,‡] J. Wolfram Wielandt,[†] Anthony C. Willis,[†] and S. Bruce Wild*[,†]

Research School of Chemistry, Australian National University, Canberra, ACT 0200, Australia and Department of Chemistry, The Faculties, Australian National University, Canberra, ACT 0200, Australia

Received May 23, 2007

Two series of triphenylphosphine-stabilized diphenyl-arsenium, -stibenium, and -bismuthenium salts of the types $[(Ph_3P)EPh_2]PF_6$ (where E = As, Sb, Bi) and $[(Ph_3P)_2EPh_2]PF_6$ (where E = Sb, Bi) have been synthesized and their structures and bonding investigated by X-ray crystallography and density functional theory at the PBE/TZP level. The coordination geometries around the central group 15 elements are distorted trigonal pyramidal in the mono(triphenylphosphine) complexes and distorted trigonal bipyramidal in the bis(triphenylphosphine) complexes, where in each case the stereochemically active lone pair of the six-electron, angular diphenyl-arsenium, -stibenium, or -bismuthenium ion occupies an equatorial position in the trigonal plane containing the C−E−C bonds. For the complexes $[(Ph_3P)EPh_2]PF_6$ (E = As, Sb, Bi), the theoretical results for the cations are consistent with the dative covalent formulation $[Ph_3P{\rightarrow}EPh_2]^+$, especially for E = As and Sb, but for $[(Ph_3P)_2EPh_2]PF_6$ (E = Sb, Bi) the bonding between the phosphines and the stibenium or bisthmuthenium ion is best described as an induced dipole−ion interaction.

Introduction

Diorgano-phosphenium, -arsenium, and -stibenium ions form stable adducts of the type $L{\rightarrow}ER_2^+X^-$, $[(L)ER_2]X$ (E = P, As, Sb) in which the two-electron ligand (L) occupies a coordination site orthogonal to the trigonal plane of the six-electron ER_2^+ group. When L is a tertiary phosphine, these main-group coordination compounds resemble labile transition-metal complexes in undergoing intermolecular ligand exchange and substitution reactions. The first complexes of this type to be isolated, $[(Et_3P)AsMe_2]Cl$, $[(Me_2PhP)AsMe_2]Cl$, and $[(Me_2PhP)SbPh_2]Cl$, were prepared by phosphine substitution of chloride in chloro-dimethylarsine or -diphenylstibine in an appropriate solvent.[1a] Addition of aqueous potassium iodide to an aqueous solution of $[(Me_2PhP)AsMe_2]Cl$ gave the iodide.[1b] Although originally considered as arsinophosphonium salts, viz. $Me_2As{-}PR_3^+X^-$, the phosphine-stabilized arsenium salt formulation, $R_3P{\rightarrow}AsMe_2^+X^-$, is consistent with the chemical behavior of the compounds − phosphine exchange at arsenic by more basic phosphines and pyridine and attack at arsenic by alkoxide, phenoxide, or the *n*-butyl ion to give arsinous acid esters[1b] or tertiary arsines[2] with liberation of the phosphine.

The complexes $[(R_3P)AsR_2]PF_6$ can be conveniently prepared by a two-phase method involving treatment of a dichloromethane solution of the phosphine and a secondary iodoarsine with aqueous ammonium hexafluorophosphate.[2] The analogous phosphine-stabilized phosphenium complexes, although similarly long known,[3] are air and moisture sensitive but show, in addition to tertiary phosphine exchange,[4−6] exchange of a secondary chlorophosphine with alkynes.[4,7] A stibine-stabilized stibenium complex $[(Me_3Sb)SbMe_2][(MeSbBr_3)_2]$ was isolated from the redistribution of bromodimethylstibine and structurally characterized.[8]

Here we describe the synthesis, structural characterization, and bonding in triphenylphosphine-stabilized arsenium, stibenium, and bismuthenium complexes of the types $[(Ph_3P)EPh_2]PF_6$ (E = As, Sb, Bi) and $[(Ph_3P)_2EPh_2]PF_6$ (E = Sb, Bi). The complex $[(Ph_3P)PPh_2]OTf$ (OTf = CF_3SO_3) has been previously isolated and structurally characterized,[6] but complexes of the diphenylarsenium ion could not be isolated.[9] The structures of these compounds are of interest because of our recent discovery that $[(Me_3P)SbPh_2]PF_6$ forms air- and water-stable halide complexes of the type $[\{(Me_3P)SbPh_2\}_4X](PF_6)_3$ (X = Cl, Br) in which the halide ions are surrounded in each case by four phosphine-stabilized stibenium ions in a square planar arrangement; attractive edge-to-face interactions between the two sets of four phenyl groups above and below the square plane containing the halide ion appear to be the main stabilizing forces in these supramolecular structures.[10]

* To whom correspondence should be addressed. E-mail: sbw@rsc.anu.edu.au (S.B.W.); rob.stranger@anu.edu.au (R.S.).

[†] Research School of Chemistry.

[‡] Department of Chemistry.

(1) (a) Coates, G. E.; Livingstone, J. G. *Chem. Ind.* **1958**, 1366. (b) Braddock, J. M. F.; Coates, G. E. *J. Chem. Soc.* **1961**, 3208−3211.

(2) Porter, K. A.; Willis, A. C.; Zank, J.; Wild, S. B. *Inorg. Chem.* **2002**, *41*, 6380−6386.

(3) (a) Issleib, K.; Seidel, W. *Chem. Ber.* **1959**, *92*, 2681−2694. (b) Nöth, H. *Z. Naturforsch.* **1960**, *15B*, 327−329.

(4) Hockless, D. C. R.; McDonald, M. A.; Pabel, M.; Wild, S. B. *J. Organomet. Chem.* **1997**, *529*, 189−196.

(5) (a) Shagvaleev, F. S.; Zykova, T. V.; Tarasova, R. I.; Sitdikova, T. S.; Moskva, V. V. *J. Gen. Chem. USSR* **1990**, *60*, 1585−1589. (b) Burford, N.; Losier, P.; Sereda, S. V.; Cameron, T. S.; Wu, G. *J. Am. Chem. Soc.* **1994**, *116*, 6474−6475.

(6) (a) Burford, N.; Cameron, T. S.; Ragogna, P. J.; Ocando-Mavarez, E.; Gee, M.; McDonald, R.; Wasylishen, R. E. *J. Am. Chem. Soc.* **2001**, *123*, 7947−7948. (b) Burford, N.; Ragogna, P. J.; McDonald, R.; Ferguson, M. J. *J. Am. Chem. Soc.* **2003**, *125*, 14404−14410.

(7) Brasch, N. E.; Hamilton, I. G.; Krenske, E. H.; Wild, S. B. *Organometallics* **2004**, *23*, 299−302.

(8) Althaus, H.; Breunig, H. J.; Lork, E. *Chem. Commun.* **1999**, 1971−1972.

(9) Burford, N.; Ragogna, P. J.; Sharp, K.; McDonald, R.; Ferguson, M. J. *Inorg. Chem.* **2005**, *44*, 9453−9460.

10.1021/om700512h CCC: $37.00
Publication on Web 11/01/2007

Table 1. Crystallographic Data and Experimental Parameters for X-ray Structural Analyses

	$[(Ph_3P)AsPh_2]PF_6$	$[(Ph_3P)SbPh_2]PF_6 \cdot CH_2Cl_2$	$[(Ph_3P)_2SbPh_2]PF_6$	$[(Ph_3P)_2BiPh_2]PF_6$
empirical formula	$C_{30}H_{25}AsF_6P_2$	$C_{31}H_{27}Cl_2F_6P_2Sb$	$C_{48}H_{40}F_6P_3Sb$	$C_{48}H_{40}BiF_6P_3$
fw, g mol^{-1}	636.39	768.15	945.50	1032.73
cryst syst	monoclinic	monoclinic	monoclinic	monoclinic
space group	$P2_1/c$	$P2_1/a$	Cc	Cc
a, Å	14.7413(2)	11.0590(2)	13.6686(1)	13.6442(3)
b, Å	11.0799(1)	18.6029(4)	14.7131(2)	14.6791(4)
c, Å	18.0760(2)	15.0804(3)	21.1858(2)	21.3363(4)
β, deg	110.357(1)	91.052(1)	93.7665(5)	92.0761(14)
V, Å^3	2768.00(6)	3102.0(1)	4251.42(8)	4270.53(17)
Z	4	4	4	4
D_{calcd}, g cm^{-3}	1.527	1.645	1.477	1.606
cryst size, mm	0.45 × 0.20 × 0.06	0.39 × 0.11 × 0.06	0.40 × 0.27 × 0.18	0.48 × 0.27 × 0.16
μ, mm^{-1}	1.403	1.222	0.822	4.301
instrument	Nonius Kappa CCD	Nonius Kappa CCD	Nonius Kappa CCD	Nonius Kappa CCD
radiation	Mo Kα	Mo Kα	Mo Kα	Mo Kα
no. of unique reflns	8050	6113	12 411	9197
no. of reflns obsd ($I > 3\sigma(I)$)	4223	3310	8111	6717
temp, K	200	200	200	200
struct refinement	CRYSTALS[29]	CRYSTALS[29]	CRYSTALS[29]	CRYSTALS[29]
final R_1, wR_2	0.0280, 0.0301	0.0335, 0.0388	0.0256, 0.0278	0.0447, 0.0511

Results and Discussion

Syntheses and Crystal Structures. The complexes $[(Ph_3P)EPh_2]PF_6$ (E = As, Sb, Bi) and $[(Ph_3P)_2EPh_2]PF_6$ (E = Sb, Bi) were prepared by addition of a dichloromethane solution of the chlorodiphenyl-arsine, -stibine, or -bismuthine to a solution of triphenylphosphine in the same solvent to which thallium(I) hexafluorophosphate had been added (eqs 1 and 2).

$$Ph_3P + Ph_2ECl \xrightarrow[-TlCl]{TlPF_6} [(Ph_3P)EPh_2]PF_6 \quad (E = As, Sb, Bi) \quad (1)$$

$$2Ph_3P + Ph_2ECl \xrightarrow[-TlCl]{TlPF_6} [(Ph_3P)_2EPh_2]PF_6 \quad (E = Sb, Bi) \quad (2)$$

The complexes were isolated as colorless solids from the reaction mixtures by evaporation of the dichloromethane after removal of thallium(I) chloride and excess thallium(I) hexafluorophosphate by filtration. Recrystallization of the crude products from dichloromethane by addition of diethyl ether gave the pure complexes as colorless crystals. Crystal data, information relating to data collection, and refinement details for the four complexes are given in Table 1. The complex $[(Ph_3P)AsPh_2]PF_6$ crystallizes in the monoclinic space group $P2_1/c$ with four molecules in the unit cell. The structure is shown in Figure 1, and important distances and angles in the cation of the salt are given in Table 2. Prominent features of the structure of the cation are as follows: (a) the P−As distance of 2.3555(6) Å is longer than the sum of the covalent radii of the two elements, viz. 2.29 Å,[11] and compares closely with the corresponding distance in $[(Ph_3P)AsMePh]PF_6$, 2.3480(5) Å; (b) the C−As−C angle in the angular Ph_2As^+ group of 105.11(9)° is also similar to the corresponding angle in the $PhMeAs^+$ complex,[2] although in the former structure there is a significant twist between the planes of the two phenyl groups, as evidenced by the dihedral angle of 173.7(2)° (C12−C11−As1−C21); and (c) the angles P1−As1−C11 and P1−As1−C21 are 99.89(6)° and 97.98(6)°, respectively, which allows the coordination geometry around the arsenic to be described as a distorted trigonal pyramid in which the angular six-electron AsC_2 group of atoms and the lone pair of electrons occupies the base and the phosphorus the apex. Because of the chirality generated in the molecule by the twisted arrangement of the two phenyl rings of the arsenium ion, there are two molecules of each enantiomer (atropisomer) related by an inversion center in the centrosymmetrical unit cell of the crystal. The structure of the cation is similar to that of the cation of $[(Ph_3P)PPh_2]OTf$, where a significant dihedral displacement between the planes of the phenyl groups on the phosphenium ion is also found in the crystal structure of the complex.[6] In the cation of $[(Ph_3P)AsMePh]PF_6$, the carbon atoms of the methyl group and the phenyl groups are coplanar within 0.192 Å.[2]

The salt $[(Ph_3P)SbPh_2]PF_6 \cdot CH_2Cl_2$ crystallizes in the monoclinic space group $P2_1/a$ with four molecules in the unit cell (Table 1). The structure of the cation is similar to that of the arsenic analogue shown in Figure 1. Important bond distances and angles in the structure are given in Table 2. The P−Sb distance of 2.5950(12) Å in the cation of the complex compares with the distance of 2.50 Å for the sum of the covalent radii.[11] The structure is very similar to that of the arsenic analogue, although in the antimony complex the angles subtended by the phosphorus to the ipso carbon atoms of the phenyl rings are closer to 90°. The dihedral angle between the planes of the phenyl groups of the stibenium ion is 172.6(3)° (C12−C11−As1−C21), and there are two inversion-related pairs of each

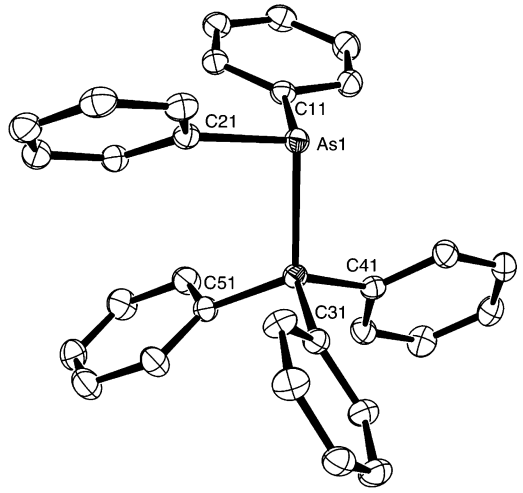

Figure 1. Displacement ellipsoid diagram for the cation of $[(Ph_3P)AsPh_2]PF_6$ showing 30% probability ellipsoids for non-hydrogen atoms.

(10) Wielandt, J. W.; Kilah, N. L.; Willis, A. C.; Wild, S. B. *Chem. Commun.* **2006**, 3679−3680.

(11) Blom, R.; Haaland, A. *J. Mol. Struct.* **1985**, *128*, 21−27.

Table 2. Selected Bond Distances (Å) and Angles (deg) in the Complexes

	$[(Ph_3P)AsPh_2]PF_6$	$[(Ph_3P)SbPh_2]PF_6 \cdot CH_2Cl_2$	$[(Ph_3P)_2SbPh_2]PF_6$	$[(Ph_3P)_2BiPh_2]PF_6$
E1−P1	2.3555(6)	2.5950(12)	2.8694(8)	2.968(3)
E1−P11			2.8426(9)	2.937(3)
E1−C11	1.961(2)	2.152(5)	2.157(2)	2.265(8)
E1−C21	1.957(2)	2.153(5)	2.157(3)	2.214(10)
P1−C31	1.805(2)	1.805(5)	1.814(3)	1.812(12)
P1−C41	1.800(2)	1.794(4)	1.827(4)	1.833(11)
P1−C51	1.798(2)	1.805(4)	1.807(4)	1.812(12)
P11−C131			1.820(4)	1.811(12)
P11−C141			1.816(4)	1.815(12)
P11−C151			1.824(4)	1.817(11)
P1−E1−C11	99.89(6)	93.70(12)	87.88(7)	87.9(2)
P1−E1−C21	97.98(6)	97.61(12)	86.58(10)	86.9(3)
P11−E1−C11			86.67(7)	86.5(2)
P11−E1−C21			87.00(10)	86.2(3)
C11−E1−C21	105.11(9)	100.14(18)	102.46(11)	101.1(3)
P1−E1−P11			170.49(2)	170.11(8)
E1−P1−C31	106.29(7)	109.61(15)	111.06(11)	111.4(4)
E1−P1−C41	108.18(7)	107.28(14)	109.38(11)	110.1(3)
E1−P1−C51	116.25(7)	115.72(14)	117.57(12)	117.2(4)
E1−P11−C131			111.47(12)	112.6(4)
E1−P11−C141			120.40(12)	119.2(4)
E1−P11−C151			105.82(11)	106.2(3)
C12−C11−E1−C21	173.7(2)	172.6(3)	−156.6(2)	−156.1(7)

atropisomer of the molecule in the unit cell. In the square-planar halide complexes $[\{(Me_3P)SbPh_2\}_4X](PF_6)_3$ (X = Cl, Br), the cations have C_{4h} symmetry and the relatively small dihedral displacements between the planes of the phenyl groups on each antimony, 23.98°, allow the phenyl groups on adjacent stibenium groups to interact with one another in attractive edge-to-face arrays above and below the square planes of the Sb_4X cores.[10]

The complexes $[(Ph_3P)_2SbPh_2]PF_6$ and $[(Ph_3P)_2BiPh_2]PF_6$ are isomorphous and crystallize in the space group *Cc* with four molecules in the unit cell (Table 1). The structure of the cation of the Sb complex is shown in Figure 2. Important distances and angles in the cations are listed in Table 2. Both structures have geometries around the central atoms that are based on the trigonal bipyramid, where in each case one equatorial site is vacant in the trigonal plane of the angular, six-electron diphenylstibenium or diphenylbismuthenium group and the phosphorus atoms occupy the apical positions. The Sb−P distances of 2.8694(8) and 2.8426(9) Å in the bis(triphenylphosphine)-stibenium complex are considerably longer than the corresponding distance in the cation of $[(Ph_3P)SbPh_2]PF_6$, viz. 2.5950(12) Å, and also longer than the sum of the covalent radii (2.50 Å).[11] The P−Bi distances in the bismuthenium complex of 2.968(3) and 2.937(3) Å compare with the value of 2.64 Å for the sum of the covalent radii.[11] The two phosphorus atoms in each complex subtend almost identical angles at antimony, 170.49(2)°, and bismuth, 170.11(8)°, but the angles subtended by the ipso carbon atoms of the two phenyl groups in the equatorial plane of each cation are considerably less than the ideal values for a trigonal bipyramid, 102.46(11)° (Sb) and 101.1(3)° (Bi). The geometries of the cations in the two compounds are those expected for 4-coordinate, 10-electron species based on valence-shell electron-pair repulsion theory and are consistent with those found in the related complexes containing ligands having hard donors, viz. $[\{(Me_2N)_3PO\}_2BiPh_2]BF_4$,[12,13] $[\{(Me_2N)_3PO\}_2BiPh_2]PF_6$, $[\{(Me_2N)_2PO\}_2BiMes_2]PF_6$, and $[(Ph_3PO)_2BiPh_2]PF_6$,[13] and $[\{(Me_2N)_3PO\}_2BiPh_2]BF_4$ that is absent in $[(Ph_3PO)_2BiPh_2]BF_4$.[14] The compounds $[(Ph_3AsO)_2BiPh_2]ClO_4$,[15] $[py_2BiPh_2]X$ (X = BF_4, PF_6), and $[(Ph_3PO)_2BiMes_2]PF_6$ have also been isolated[13] but not been structurally characterized by X-ray crystallography. The complex $[\{(Me_2N)_3PO\}_2BiPh_2]OTf$ and related aryl derivatives have been prepared by adding Me_3SiOTf to a dichloromethane solution of the appropriate diarylbismuth chloride and the phosphoramide.[16] Use of these complexes for the synthesis of unsymmetrically substituted bismuthines by addition of Grignard reagents was found to be more expedient than the use of moisture-sensitive, diarylbismuth halides, which are difficult to obtain in high purity.

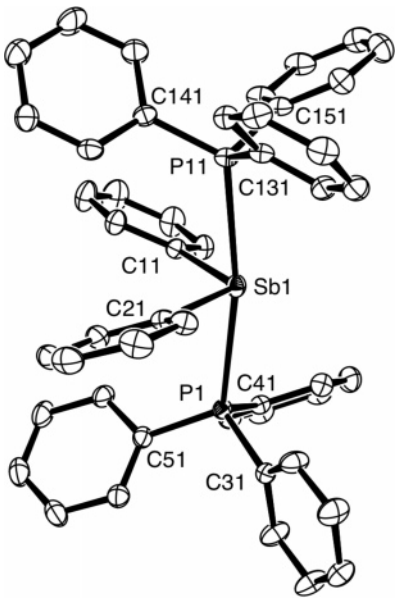

Figure 2. Displacement ellipsoid diagram for the cation of $[(Ph_3P)_2SbPh_2]PF_6$ showing 30% probability ellipsoids for non-hydrogen atoms.

NMR Spectroscopy. Complexes of the type $[(R_3P)EPh_2]X$ undergo rapid ligand exchange in solution.[2,4−6] Similar dissociative exchange of triphenylphosphine appears to occur in solution for complexes $[(Ph_3P)EPh_2]PF_6$ (E = As, Sb, Bi) and $[(Ph_3P)_2EPh_2]PF_6$ (E = Sb, Bi). Ligand exchange is indicated

(12) Carmalt, C. J.; Norman, N. C.; Orpen, A. G.; Stratford, S. E. *J. Organomet. Chem.* **1993**, *460*, C22−C24.
(13) Carmalt, C. J.; Farrugia, L. J.; Norman, N. C. *J. Chem. Soc., Dalton Trans.* **1996**, 443−454.
(14) Carmalt, C. J.; Walsh, D.; Cowley, A. H.; Norman, N. C. *Organometallics* **1997**, *16*, 3597−3600.
(15) Allman, T.; Goel, R. G.; Prasad, H. S. *J. Organomet. Chem.* **1979**, *166*, 365−371.
(16) Matano, Y.; Miyamatsu, T.; Suzuki, H. *Organometallics* **1996**, *15*, 1951−1953.

Table 3. Comparisons of Optimized Geometries for $[(Ph_3P)EPh_2]^+$ with Crystal Structure Data

	E = P			E = As			E = Sb			E = Bi	
	calcd[a]	calcd[b]	XRD[c]	calcd[a]	calcd[b]	XRD[d]	calcd[a]	calcd[b]	XRD[d]	calcd[a]	calcd[b]
E−P (Å)	2.243	2.235	2.230	2.390	2.386	2.356	2.626	2.618	2.595	2.755	2.723
C−E (Å)[e]	1.859(1)	1.854(1)	1.837	2.002(1)	1.998(1)	1.959	2.193(4)	2.192(2)	2.153	2.299(6)	2.293(6)
C11−E−C21 (deg)	105.7	105.8	104.3	101.3	101.3	105.1	98.5	98.3	100.1	95.6	96.1
C−E−P (deg)	106.1(6)	106.0(6)	100.6	103.2(4)	103.1(3)	98.9	101.5(8)	101.5(7)	95.7	97.2(0)	98.9(1)
C−P (Å)[f]	1.825(2)	1.821(4)	1.808	1.824(2)	1.819(2)	1.802	1.822(2)	1.817(2)	1.801	1.825(2)	1.819(2)

[a] Geometry optimized without relativistic corrections. [b] Geometry optimized with scalar relativistic corrections. [c] Literature data for $[(Ph_3P)PPh_2]OTf$.[6a] [d] This work. [e] Average of two nonidentical values. [f] Average of three nonidentical values.

Table 4. Comparisons of Optimized Geometries for $[(Ph_3P)_2EPh_2]^+$ with Crystal Structure Data

	E = As		E = Sb			E = Bi		
	calcd[a]	calcd[b]	calcd[a]	calcd[b]	X-ray	calcd[a]	calcd[b]	X-ray
E−P11 (Å)	2.702	2.701	2.909	2.907	2.843	3.012	3.012	2.937
E−P1 (Å)	2.834	2.777	2.929	2.912	2.869	3.018	3.013	2.968
C−E (Å)[c]	1.987(2)	1.984(1)	2.182(1)	2.179(2)	2.157	2.291(3)	2.280(1)	2.240
C11−E−C21 (deg)	109.7	106.3	106.0	102.6	102.5	104.1	100.9	101.1
C−E−P11 (deg)[c]	91.3(9)	91.9(8)	89.9(6)	91.0(1)	86.8	87.7(1)	90.6(1)	86.4
C−P11 (Å)[d]	1.833(4)	1.827(2)	1.831(2)	1.825(1)	1.820	1.837(5)	1.827(1)	1.814
C−E−P1 (deg)[c]	89.9(5)	91.5(1.5)	90.2(2)	91.4(6)	87.2	87.5(8)	90.7(2)	87.4
C−P1 (Å)[d]	1.842(5)	1.831(1)	1.837(8)	1.827(2)	1.816	1.832(6)	1.829(2)	1.819
P11−E−P1 (deg)[c]	177.9	174.4	179.4	176.0	170.5	172.2	178.0	170.1

[a] Geometry optimized without relativistic corrections. [b] Geometry optimized with scalar relativistic corrections. [c] Average of two values. [d] Average of three values.

by the appearance of the resonances for phosphorus nuclei in the complexes, which are broad and of similar chemical shift for $[(Ph_3P)EPh_2]PF_6$ and $[(Ph_3P)_2EPh_2]PF_6$ (E = Sb, Bi). Variable-temperature ^{31}P NMR spectroscopic measurements were conducted on CD_2Cl_2 solutions of $[(Ph_3P)SbPh_2]PF_6$ and $[(Ph_3P)_2SbPh_2]PF_6$ in the range 25 and −90 °C; a small decrease in the broadening of the signals was apparent on cooling below 0 °C. Small differences in the values of the chemical shifts for the phosphorus nuclei were also observed for both series of complexes as the temperature of the solutions was reduced to −90 °C.

Density Functional Theory (DFT) Calculations. *Isolation of Stationary Points.* Calculations of the structures of $[(Ph_3P)EPh_2]^+$ and $[(Ph_3P)_2EPh_2]^+$ (E = As, Sb, Bi) in the absence of symmetry constraints and relativistic corrections yield optimized geometries that conform well with the structures determined by X-ray crystallography. Similar calculations on the cation of $[(Ph_3P)PPh_2]OTf$, for which the crystal structure has been reported,[6a] also show good agreement with experiment. A comparison of the key bond lengths and angles in the cations is given in Tables 3 and 4. In each case, the calculated bond lengths are slightly longer than the crystallographic values with the largest discrepancies being for the long E−P bonds in $[(Ph_3P)_2EPh_2]^+$. The bond length increases found at the PBE/TZP level (E−P bond length increases in the range 0.044 ± 0.031 Å) are consistent with the performance of this method on other compounds containing the heavier group 15 elements.[17] When scalar relativistic corrections are included,[18] the calculated bond lengths for the complexes still exceed the crystal structure values but generally by smaller margins. The strongest apparent influence is on the lengths of the E−P, E−C, and P−C bonds, which contract when relativistic effects are included. It is generally accepted that relativistic corrections, although comparatively unimportant for bonds between first- and second-row atoms, become significant with increasing nuclear charge. Consistent with this expectation, the treatment of relativistic effects in $[(Ph_3P)EPh_2]^+$ has the greatest impact for the bismuthenium complex, where the Bi−P bond length decreases by 0.028 Å. In the adducts $[(Ph_3P)_2EPh_2]^+$, however, the most dramatic reduction occurs in the arsenium complex, where one E−P bond is 0.057 Å shorter; the E−P bond contractions in the stibenium and bismuthenium complexes are progressively more modest. The overall reductions in the calculated E−P bond lengths for the complexes bring these quantities to within 0.047 Å of the crystallographic values when relativistic corrections are included.

The following points of comparison between the structures are instructive. (a) For E = As, Sb, or Bi, the E−P bonds in $[(Ph_3P)EPh_2]^+$ are consistently at least 0.25 Å shorter than either of the E−P distances in $[(Ph_3P)_2EPh_2]^+$. For example, at the PBE/TZP level, r(Sb−P1) in $[(Ph_3P)SbPh_2]^+$ is 2.626 Å compared to the value of 2.618 Å obtained from the relativistically corrected optimization, whereas the corresponding distances in $[(Ph_3P)_2SbPh_2]^+$ are 2.909 and 2.929 Å compared to 2.907 and 2.912 Å, respectively (mean increase of 0.293 Å compared to 0.292 Å). These increments correspond closely with the mean increase of 0.260 Å found in the E−P distances for $[(Ph_3P)SbPh_2]^+$ versus $[(Ph_3P)_2SbPh_2]^+$ by X-ray crystallography. (b) The calculated As−P distance in $[(Ph_3P)AsPh_2]^+$ is 0.236 Å (0.232 Å by the relativistically corrected optimization) shorter than the Sb−P distance in the corresponding stibenium complex, which is in excellent agreement with the 0.239 Å difference observed in the crystal structures. (c) The mean calculated Bi−P distance in $[(Ph_3P)_2BiPh_2]^+$ is 0.096 Å (versus 0.103 Å) longer than the mean calculated Sb−P distance in $[(Ph_3P)_2SbPh_2]^+$, which is almost identical to the increment of 0.098 Å found in the crystallographic determinations.

These comparisons suggest that the bond length overestimation at the PBE/TZP level of theory is sufficiently regular to inspire confidence in the method's ability to reliably predict the structures of complexes for which crystal structures are unavailable, viz. $[(Ph_3P)BiPh_2]^+$ and $[(Ph_3P)_2AsPh_2]^+$. For example, in the absence of relativistic corrections, the calculated As−P distances in $[(Ph_3P)_2AsPh_2]^+$ are 2.702 and 2.834 Å;

(17) Petrie, S.; Stranger, R.; Rae, A. D.; Willis, A. C.; Zhou, X.; Wild, S. B. *Organometallics* **2006**, *25*, 164−171.

(18) van Lenthe, E.; Baerends, E.-J.; Snijders, J. G. *J. Chem. Phys.* **1993**, *99*, 4597−4610. van Lenthe, E.; Ehlers, A. E.; Baerends, E.-J. *J. Chem. Phys.* **1999**, *110*, 8943−8953.

Table 5. Calculated BDEs (kJ mol^{-1}) for E−P Bonds in $[(Ph_3P)_iEPh_2]^+$ (i = 1, 2)

	calcd[a]	calcd[b]	calcd[c]	calcd[d]
$[(Ph_3P)PPh_2]^+$	194.7	194.5	189.8	367.8
$[(Ph_3P)AsPh_2]^+$	185.6	184.5	185.0	339.6
$[(Ph_3P)SbPh_2]^+$	185.5	182.5	181.4	301.1
$[(Ph_3P)BiPh_2]^+$	176.2	170.2	172.9	277.1
$[(Ph_3P)_2AsPh_2]^+$	62.1	62.0	79.8	82.9
$[(Ph_3P)_2SbPh_2]^+$	82.7	79.9	97.1	96.5
$[(Ph_3P)_2BiPh_2]^+$	80.1	77.3	98.6	100.4

[a] BDE (adiabatic) without relativistic correction. [b] BDE (adiabatic) with scalar relativistic corrections applied in single-point calculations on uncorrected optimized geometries. [c] BDE (adiabatic) with scalar relativistic corrections incorporated during optimization. [d] BDE (vertical) without relativistic correction and with the separated PPh_3 and (Ph_2E^+ or $[(PPh_3)EPh_2^+]$) fragments having geometries identical to those within the optimized $[(PPh_3)_iEPh_2]^+$ complex.

Table 6. Bond Energy Decomposition Values (kJ mol^{-1}) for E−P Bonds in $[(Ph_3P)_iEPh_2]^+$ (i = 1, 2)

	ΔE_{Pauli}	ΔV_{elstat}	ΔE_0	ΔE_{orbit}	$BDE_{vertical}$
$[(Ph_3P)PPh_2]^+$	958	−569	389	−757	368
$[(Ph_3P)AsPh_2]^+$	754	−494	260	−600	340
$[(Ph_3P)SbPh_2]^+$	554	−398	156	−457	301
$[(Ph_3P)BiPh_2]^+$	488	−366	121	−398	277
$[(Ph_3P)_2AsPh_2]^+$	227	−153	73	−156	83
$[(Ph_3P)_2SbPh_2]^+$	244	−175	69	−166	97
$[(Ph_3P)_2BiPh_2]^+$	230	−172	59	−159	101

Table 7. Positive Charge Distributions in $[(Ph_3P)_iEPh_2]^+$ (i = 1, 2)[a]

	q(E1, EPh_2)	q(P1, PPh_3)	q(P11, PPh_3)	q_{total}
$[(Ph_3P)PPh_2]^+$	0.434	0.573		1.007
$[(Ph_3P)AsPh_2]^+$	0.459	0.547		1.006
$[(Ph_3P)SbPh_2]^+$	0.499	0.504		1.003
$[(Ph_3P)BiPh_2]^+$	0.527	0.475		1.002
$[(Ph_3P)_2AsPh_2]^+$	0.416	0.320	0.267	1.003
$[(Ph_3P)_2SbPh_2]^+$	0.469	0.264	0.272	1.005
$[(Ph_3P)_2BiPh_2]^+$	0.480	0.263	0.264	1.007

[a] Charge distributions obtained by Hirshfeld charge analysis.

when relativistic corrections are included, the longer As−P bond contracts to 2.777 Å whereas the shorter bond is almost unchanged. Nevertheless, the calculated difference between the lengths of the two As−P bonds in the arsenium complex is much greater than either the calculated or the experimental difference between the E−P distances in $[(Ph_3P)_2SbPh_2]^+$ and $[(Ph_3P)_2BiPh_2]^+$.

Another significant difference between the structures of the complexes $[(Ph_3P)EPh_2]^+$ and $[(Ph_3P)_2EPh_2]^+$ is that the planes containing the C11−E−C21 atoms in the former complexes are tilted significantly out of perpendicularity with respect to the E−P axes, as reflected in the calculated C−E−P angles of 103° (E = As) and 102° (E = Sb), compared to the essentially perpendicular arrangement in the latter complexes, where the angles are within the range 87−92°.

Bond Strengths and Bond Decomposition Analysis. The bond dissociation energy (BDE) values for the E−PPh_3 bonds in the two series of complexes have been determined by comparison of the total energies for $[(Ph_3P)_iEPh_2]^+$ (i = 1, 2) with the sums of the total energies of the relevant optimized fragments. These values have been calculated by the following four techniques: (a) through optimization with complete exclusion of relativistic corrections; (b) through optimization excluding relativistic effects but with subsequent scalar relativistic corrections in single-point calculations; (c) through optimization including relativistic corrections; and (d) through molecular fragment-based calculations, which are described in detail below. The values obtained for the BDEs by the four methods are listed in Table 5. It should be noted that the values obtained in each case are likely overestimates of the 'true' BDEs because the calculations omit both zero-point vibrational energies and basis-set superposition error corrections. It is interesting to note, however, that for the complexes $[(Ph_3P)EPh_2]^+$ the BDEs determined by methods a−c are broadly consistent whereas for $[(Ph_3P)_2EPh_2]^+$ the 'relativistically optimized' BDEs are systematically ca. 15−20 kJ mol^{-1} greater than those obtained using structures optimized in the absence of relativistic corrections.

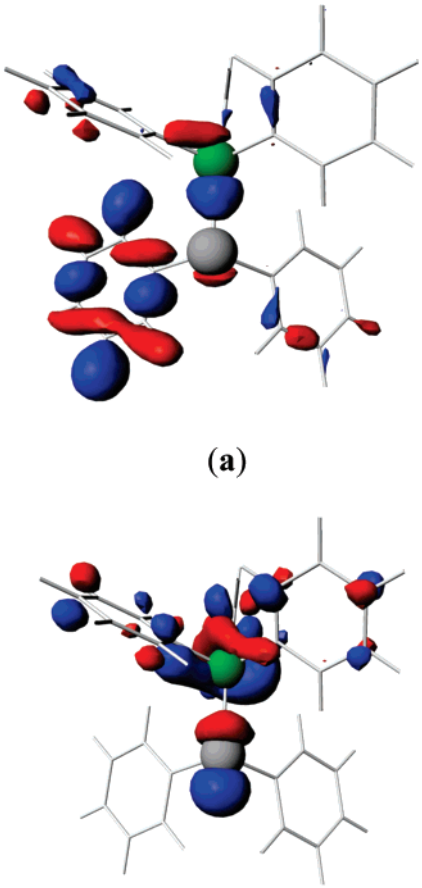

Figure 3. Molecular orbital isosurface depictions at the 0.04 density level for orbital a_{70} (filled) (*a*) and orbital a_{84} (virtual, 2LUMO) (*b*) of $[(Ph_3P)AsPh_2]^+$. The surfaces shown were generated from nonrelativistic PBE/TZP calculations using the 'small' frozen core settings for C, P, and As atoms.

The molecular-fragment-based calculations involve the subdivision of the optimized structures for $[(Ph_3P)EPh_2]^+$ or $[(Ph_3P)_2EPh_2]^+$ into fragments, for example, Ph_2E^+ and PPh_3, which are themselves frozen at the geometries optimized within the overall structures. This approach provides 'vertical' bond strengths, as opposed to the 'adiabatic' values furnished when the subunits are independently optimized. During the fragment-based calculations, bond decomposition analyses were also performed.[19,20] The contributions to the strengths of the E−P bonds, as determined by the calculations, are given in Table 6. The bond decomposition analyses for $[(Ph_3P)EPh_2]^+$ indicate

(19) Morokuma, K. *J. Chem. Phys.* **1971**, *55*, 1236−1244. Kitaura, K.; Morokuma, K. *Int. J. Quantum Chem.* **1976**, *10*, 325−340. Bickelhaupt, F. M.; Baerends, E. J. In *Reviews in Computational Chemistry*; Lipkowitz, K. B., Boyd, D. B., Eds.; Wiley-VCH: New York, 2000; Vol. 15, p 1.

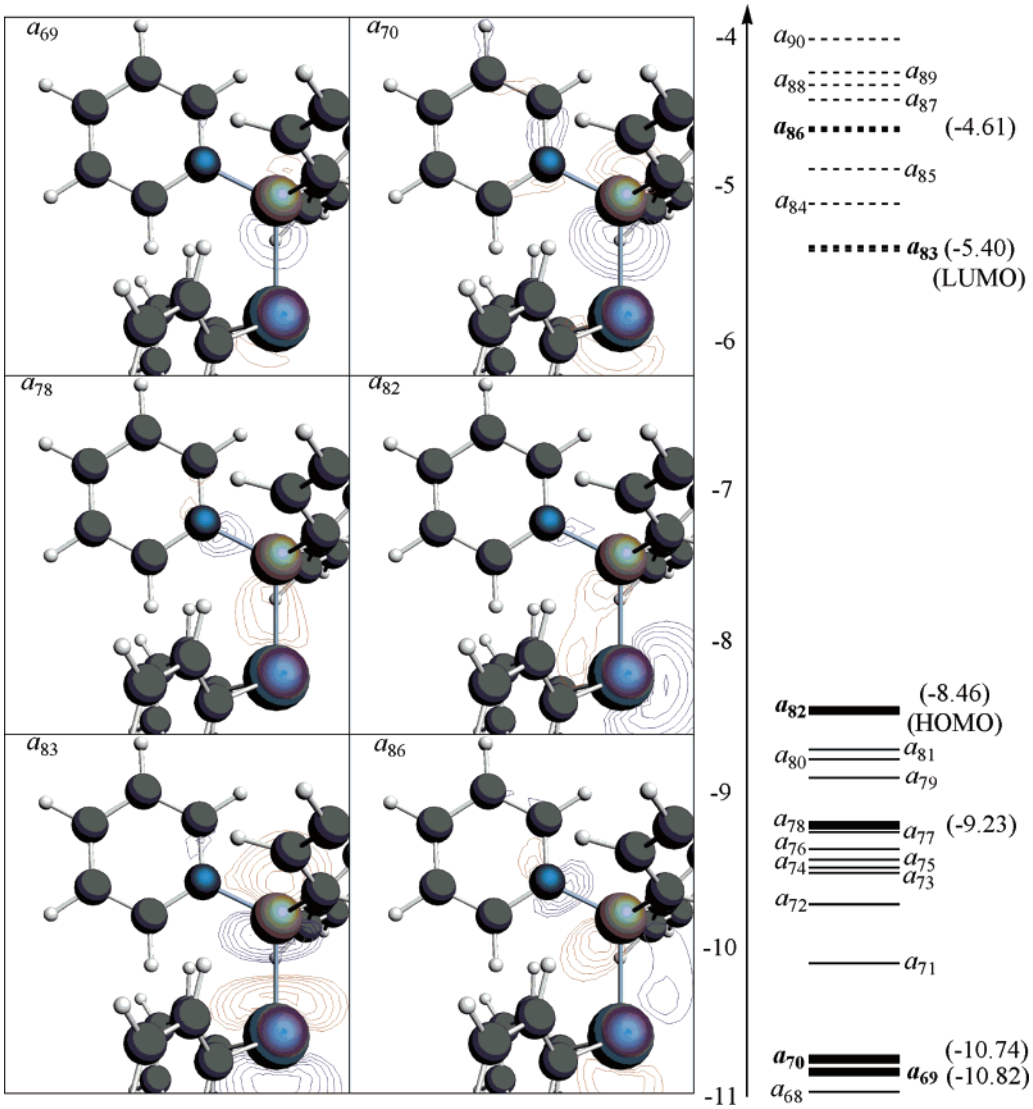

Figure 4. Molecular orbital contour plots, shown in the plane of the (highlighted) Sb, P, and C51 atoms of $[(Ph_3P)SbPh_2]^+$, where C51 is the ipso carbon of the *P*-phenyl ring that is staggered with respect to both *Sb*-phenyl rings. Contour settings are logarithmic and arbitrary (but identical for all displayed MOs, so that the relative density between P and Sb can be easily assessed for the various orbitals).

that the principal attractive component of the E−P bond is the orbital contribution ΔE_{orbit}, which exceeds the electrostatic contribution ΔV_{elstat} by 32−188 kJ mol^{-1}. For the complexes $[(Ph_3P)_2EPh_2]^+$, however, the electrostatic component is generally greater than the orbital contribution. Although the 'orbital' and 'electrostatic' components do not correspond exactly to the orthodox chemical understanding of 'covalent' and 'ionic' interactions, the trends found are consistent with an interpretation in which the complexes $[(Ph_3P)EPh_2]^+$ are held together by essentially covalent P→E bonds whereas $[(Ph_3P)_2EPh_2]^+$ display the character of ion−ligand complexes. These descriptions are supported by the crystallographic data, where it is seen that the Sb−P distances in $[(Ph_3P)_2SbPh_2]^+$ are longer than the corresponding distance in $[(Ph_3P)SbPh_2]^+$; this relationship between the bond lengths of the two sets of complexes is mirrored in the calculated geometries for E = As, Sb, and Bi. When the calculated geometric data for $[(Ph_3P)EPh_2]^+$ and $[(Ph_3P)_2EPh_2]^+$ are compared, it is apparent that the primary adducts possess E−P distances that are close to the sum of the covalent radii, while E−P distances in the secondary adducts substantially exceed that sum, making it difficult to reconcile the secondary adduct geometries with any form of covalent bonding.

For both $[(Ph_3P)EPh_2]^+$ and $[(Ph_3P)_2EPh_2]^+$ it is also apparent that the 'covalent' orbital contribution progressively decreases in importance relative to the 'ionic' electrostatic contribution as E moves down the group. Consistent also with this observation, Hirshfeld charge analysis of the complexes indicates a regular increase in the positive charge density on EPh_2 moving down the group for both primary and secondary adducts (Table 7). The Hirshfeld analysis also shows that the charge is evenly distributed on the E and P centers in the complexes $[(Ph_3P)EPh_2]^+$. The EPh_2 and PPh_3 groups possess between 43% and 57% of the overall positive charge in the four mono(triphenylphosphine) complexes; in the bis(triphenylphosphine) complexes, the E centers of the EPh_2 groups consistently claim the greatest fraction of the positive charge, despite there being fewer phenyl rings available for charge delocalization than for the PPh_3 ligands. In $[(Ph_3P)_2BiPh_2]^+$, the charge localized on the $BiPh_2$ group is almost twice that on either triphenylphosphine ligand, which indicates a markedly ionic interaction between the $BiPh_2^+$ group and the PPh_3 ligands.

(20) Ziegler, T.; Rauk, A. *Inorg. Chem.* **1979**, *18*, 1558−1565. Ziegler, T.; Rauk, A. *Inorg. Chem.* **1979**, *18*, 1755−1759.

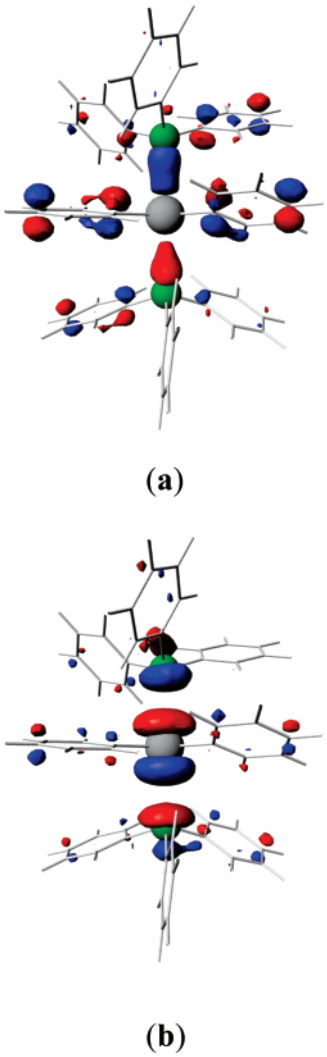

Figure 5. Molecular orbital isosurface depictions at the 0.04 density level for orbital a_{127} (filled, 2HOMO) (*a*) and orbital a_{129} (virtual, LUMO) (*b*) of $[(Ph_3P)_2SbPh_2]^+$. The surfaces shown were generated from nonrelativistic PBE/TZP calculations using the 'small' frozen core settings for C, P, and Sb atoms.

Molecular Orbital (MO) Analyses. Visualization of the orbitals for representative complexes of the types $[(Ph_3P)_iEPh_2]^+$ (i = 1, 2) indicates that the E−P bonds in each case are polar with the electron density concentrated toward the phosphine P atoms. Analysis of the E−P bonding orbital(s) is not straightforward, however, because extensive delocalization within the phenyl groups on E and P in almost all of the MOs means that no single MO exclusively represents the E−P bond. This said, the principal E−P bonding character in $[(Ph_3P)EPh_2]^+$ is typically seen in MOs that are ca. 2.2 eV below the HOMO, for example, a_{70} in $[(Ph_3P)AsPh_2]^+$ (see Figure 3). (This orbital label, and those following, refer to calculations performed without relativistic corrections, where C, P, and E were assigned 'small' frozen cores.) The a_{70} MO in $[(Ph_3P)AsPh_2]^+$ contains substantial character attributable to the triphenylphosphine lone pair (which corresponds to the HOMO in PPh_3 itself) but rather less As character. The greatest degree of As p_z character (that is, electon density aligned along the As···P axis) occurs in the 2LUMO (a_{84}) of $[(Ph_3P)AsPh_2]^+$, which possesses a compressed *P*-facing lobe and a distended opposing lobe due to the deployment of electron density from P toward As (via orbitals such as a_{70}). This combination of MO characteristics supports a description of the As−P bond in $[(Ph_3P)AsPh_2]^+$ as a polar, partially electrostatic interaction between Ph_3P and $AsPh_2^+$, influenced by ion/dipole and ion/induced dipole attractions. However, the calculated As−P bond distance of 2.39 Å in this complex (2.36 Å in crystal) indicates a partially covalent interaction, and some filled MOs do exhibit some covalent character between As and P. This is illustrated by orbitals a_{78} and a_{82} for $[(Ph_3P)SbPh_2]^+$ (Figure 4); analogous MOs are present for the As and Bi congeners. The a_{78} MO for $[(Ph_3P)SbPh_2]^+$ appears to be an almost nonpolar, covalent σ-based interaction between P and Sb, whereas the a_{82} MO displays apparent π back-donation from the Ph_2Sb^+ lone pair to P. The peak electron density between P and Sb in each of these orbitals, however, is substantially less than that extending from P to Sb in a_{70}; this observation indicates that the P−Sb interaction in the complex is markedly polar and moderately electrostatic in nature. Our conclusions for the bonding in the As and Bi congeners are similar.

The E−P bonding in $[(Ph_3P)_2EPh_2]^+$, as indicated already by the fragment-based bond decomposition analysis, is more electrostatic than in $[(Ph_3P)EPh_2]^+$. Support for this contention can be seen in the isosurface for the MO a_{127} of $[(Ph_3P)_2SbPh_2]^+$ (Figure 5). This MO is directly analogous to the weak covalent σ interaction indicated by a_{78} in $[(Ph_3P)EPh_2]^+$, but in $[(Ph_3P)_2SbPh_2]^+$ a_{127} is more localized on the P atoms than on Sb and no other filled orbitals have significant σ-interacting character on both P and Sb. We conclude that the bonding between E and P in the complexes $[(Ph_3P)EPh_2]^+$ is best described as 'electrostatic/polar covalent', but in $[(Ph_3P)_2EPh_2]^+$ it is electrostatic.

Conclusion

The complexes $[(Ph_3P)EPh_2]PF_6$ (where E = As, Sb, Bi) have structures based on the trigonal pyramid in which the EC_2 core of the six-electron diphenyl-arsenium, -stibenium, or -bismuthenium ion and the stereochemically active lone pair in each case are situated at the base with the phosphorus atom at the apex. In the complexes $[(Ph_3P)_2EPh_2]PF_6$, the phosphorus atoms occupy apical sites above and below the trigonal plane of the EC_2 core in a trigonal bipyramidal arrangement. The theoretical results indicate that the P−E interactions in $[(Ph_3P)EPh_2]PF_6$ (E = P, As, Sb) can be described as dative covalent (P→E), whereas for E = Bi, in particular, the interactions are dominated by electrostatic, induced dipole−ion attractions in both series of complexes.

Experimental Section

Solvents were purified by conventional methods and stored under nitrogen. Iododiphenylarsine,[21] chlorodiphenylstibine,[22] and chlorodiphenylbismuthine[23] were prepared according to the literature procedures. NMR spectra were recorded in dichloromethane-d_2 at 298 K on a Varian Gemini 300 spectrometer operating at 75.462 (^{13}C) and 121.47 MHz (^{31}P), with chemical shifts being referred to Me_4Si(^{13}C) and external 85% aq H_3PO_4 (^{31}P). Fast atom bombardment (FAB) mass spectra were recorded on a VG Analytical ZAB-2SEQ mass spectrometer (ionization, 30 keV Cs^+ ions) in a matrix of (2-nitrophenyl)octyl ether and dichloromethane. Elemental analyses were performed by staff within the Research School of Chemistry.

(21) Pope, W. J.; Turner, E. E. *J. Chem. Soc.* **1920**, *117*, 1447−1452.
(22) Nunn, M.; Sowerby, D. B.; Wesolek, D. M. *J. Organomet. Chem.* **1983**, *251*, C45−C46.
(23) Challenger, F.; Allpress, C. F. *J. Chem. Soc. Trans.* **1915**, *107*, 16−25.

Syntheses. A mixture of triphenylphosphine and thallium(I) hexafluorophosphate in dichloromethane (30 mL) was treated with a solution of the halodiphenyl-arsine, -stibine, or -bismuthine in dichloromethane (10 mL). A milky suspension of thallium(I) halide formed. After being stirred for ca. 1 h, the mixture was filtered and the solvent evaporated from the filtrate to give the crude product as a colorless solid, which was purified by recrystallization from dichloromethane−diethyl ether.

(Triphenylphosphine-*P*)diphenylarsenium Hexafluorophosphate. Iododiphenylarsine (1.43 g, 4.01 mmol), triphenylphosphine (1.05 g, 4.01 mmol), and thallium(I) hexafluorophosphate (1.47 g, 4.21 mmol) were used. Yield: 1.53 g (60%); mp 220 °C dec. Anal. Calcd for $C_{30}H_{25}AsF_6P_2$:C, 56.6; H, 4.0. Found: C, 56.9; H, 4.1. $^{13}C\{^1H\}$ NMR: δ 129.0 (d, $^1J_{CP} = 20.5$ Hz, C_{ipso} of PPh_3), 130.6 (s, C_{ortho} of Ph_2As^+), 130.9 (d, $^2J_{CP} = 12.5$ Hz, C_{ortho} of PPh_3), 132.5 (s, C_{para} of Ph_2As^+), 134.3 (d, $^3J_{CP} = 9.1$ Hz, C_{meta} of PPh_3), 135.1 (s, C_{meta} of Ph_2As^+), 135.6 (d, $^4J_{CP} = 3.3$ Hz, C_{para} of PPh_3). $^{31}P\{^1H\}$ NMR: δ −143.9 (septet, $^1J_{PF} = 709.9$ Hz, PF_6), 13.6 (s, PPh_3). FAB MS: *m*/*z* 491 amu ($[M]^+$, 25%).

(Triphenylphosphine-*P*)diphenylstibenium Hexafluorophosphate 1-Dichloromethane. Chlorodiphenylstibine (0.55 g, 1.78 mmol), triphenylphosphine (0.47 g, 1.78 mmol), and thallium(I) hexafluorophosphate (0.64 g, 1.84 mmol) were used. Yield: 0.55 g (40%); mp 147 °C dec. Anal. Calcd $C_{31}H_{27}Cl_2F_6P_2Sb$: C, 48.5; H, 3.5. Found: C, 49.0; H, 3.5. $^{13}C\{^1H\}$ NMR: δ 127.4 (d, $^1J_{CP} = 23.8$ Hz, C_{ipso} of PPh_3), 129.4 (d, $^2J_{CP} = 8.0$ Hz, C_{ortho} of PPh_3), 129.8 (s, C_{meta} of Ph_2Sb^+), 130.6 (s, C_{para} of Ph_2Sb^+), 130.9 (s, C_{para} of PPh_3), 133.7 (d, $^3J_{CP} = 14.6$ Hz, C_{meta} of PPh_3), 136.2 (s, C_{ortho} of Ph_2Sb^+), 139.1 (s, C_{ipso} of Ph_2Sb^+). $^{31}P\{^1H\}$ NMR: δ −143.7 (septet, $^1J_{PF} = 711.4$ Hz, PF_6), −4.2 (s, PPh_3). FAB MS: *m*/*z* 537 amu ($[M]^+$, 100%).

(Triphenylphosphine-*P*)diphenylbismuthenium Hexafluorophosphate 1-Dichloromethane. Chlorodiphenylbismuthine (0.94 g, 2.36 mmol), triphenylphosphine (0.62 g, 2.36 mmol), and thallium(I) hexafluorophosphate (0.86 g, 2.47 mmol) were used. Yield: 0.91 g (50%); mp 177 °C dec. Anal. Calcd for $C_{31}H_{27}BiCl_2F_6P_2$: C, 43.5; H, 3.2. Found: C, 43.8; H, 3.2. $^{13}C\{^1H\}$ NMR: δ 124.5 (d, $^1J_{CP} = 37.4$ Hz, C_{ipso} of PPh_3), 130.0 (d, $^3J_{CP} = 10.6$ Hz, C_{meta} of PPh_3), 130.3 (s, C_{para} of PPh_3), 132.6 (s, C_{meta} of Ph_2Bi^+), 133.2 (s, C_{para} of Ph_2Bi^+), 133.9 (d, $^2J_{CP} = 11.1$ Hz, C_{ortho} of PPh_3), 138.4 (s, C_{ortho} of Ph_2Bi^+). $^{31}P\{^1H\}$ NMR: δ −143.6 (septet, $^1J_{PF} = 713.6$ Hz, PF_6), −3.9 (s, PPh_3). FAB MS: *m*/*z* 625 amu ($[M]^+$, 100%).

Bis(triphenylphosphine-*P*)diphenylstibenium Hexafluorophosphate. Chlorodiphenylstibine (0.65 g, 2.07 mmol), triphenylphosphine (1.09 g, 4.15 mmol), and thallium(I) hexafluorophosphate (0.76 g, 2.16 mmol) were used. Yield: 0.98 g (50%); mp 157 °C dec. Anal. Calcd for $C_{48}H_{40}F_6P_3Sb$: C, 61.0; H, 4.3. Found: C, 60.4; H, 4.4. $^{13}C\{^1H\}$ NMR: δ 130.6 (br, C_{ortho} of PPh_3, C_{meta} of Ph_2Sb^+), 131.9 (s, C_{para} of Ph_2Sb^+), 134.1 (br, C_{meta} of PPh_3), 135.6 (s, C_{ortho} of Ph_2Sb^+), 137.2 (s, C_{para} of PPh_3). $^{31}P\{^1H\}$ NMR: δ −143.7 (septet, $^1J_{PF} = 712.5$ Hz, PF_6), −4.5 (br, PPh_3). FAB MS: *m*/*z* 537 amu ($[M - PPh_3]^+$, 100%).

Bis(triphenylphosphine-*P*)diphenylbismuthenium Hexafluorophosphate. Chlorodiphenylbismuthine (0.74 g, 1.86 mmol), triphenylphosphine (0.97 g, 3.72 mmol), and thallium(I) hexafluorophosphate (0.68 g, 1.96 mmol) were used. Yield: 0.91 g (50%); mp 188 °C dec. Anal. Calcd for $C_{48}H_{40}BiF_6P_3$: C, 55.7; H, 3.9. Found: C, 55.8; H, 3.9. $^{31}P\{^1H\}$ NMR: δ −143.4 (septet, $^1J_{PF} = 714.9$ Hz, PF_6), −4.21 (br, PPh_3). FAB MS: *m*/*z* 625 amu ($[M^+ - PPh_3]^+$, 60%); 262 amu ($[PPh_3]^+$, 100%). A quantity of (triphenylphosphine-*P*)diphenylbismuthenium hexafluorophosphate was isolated from the filtrate. Yield: 0.40 g (25%).

Theoretical Methods. Density functional theory calculations were performed on Linux-based Pentium computers and in parallel mode on the SGI Altix AC supercomputer operated by the Australian Partnership for Advanced Computing (APAC). Calculations were carried out with use of the Amsterdam Density Functional (ADF) program, version ADF2004.01,[24] and employed the Perdew−Burke−Ernzerhof (PBE) gradient-corrected functional[25] with small-core, Slater-orbital basis sets of triple-ζ plus polarization (TZP) quality. Previous calculations on a series of diiodomethyl- and diiodophenyl-arsine−tertiary arsine adducts indicated that the PBE functional performs well in modeling the bonding between group 15 atoms.[17] Optimized geometries were obtained, both with and without ZORA scalar relativistic corrections,[18] using the gradient algorithm of Versluis and Ziegler.[26] Energy, gradient, and displacement cutoffs for the optimizations were set a factor of 2 tighter than the ADF defaults to improve the reliability of the optimized structures. Further single-point calculations used a fragment-based approach to characterize contributions to the E−P bond of interest. Vibrational frequency calculations for the species surveyed here were not pursued. Note that a principal purpose of frequency calculations is to probe whether any stationary points found are genuine minima. In the present instance, where all of the optimized stationary points were observed to be markedly asymmetric and since unconstrained asymmetric stationary points located through energy minimization are almost without exception minima, it was not judged necessary or desirable to perform lengthy frequency calculations on these large asymmetric structures. All calculations were performed in a spin-restricted fashion and in the absence of symmetry constraints.

Crystal Structures. Crystallographic data and experimental parameters for the X-ray structural analyses are given in Table 1. Data were processed using Denzo and Scalepack software and corrected for absorption by the Gaussian integration method implemented in maXus.[27] The structures were solved by direct methods (SIR92)[28] and refined by full matrix on *F* with use of CRYSTALS.[29] All non-hydrogen atoms were refined with anisotropic displacement parameters. Hydrogen atoms were included at calculated positions and allowed to ride on the atoms to which they are attached. Molecular graphics were produced with ORTEP-3.[30]

Acknowledgment. R.S. and S.B.W. gratefully acknowledge the Australian Research Council (ARC) for financial support.

Supporting Information Available: Crystallographic data for the four complexes (CIF). This material is available free of charge via the Internet at http://pubs.acs.org.

OM700512H

(24) Fonseca Guerra, C.; Snijders, J. G.; te Velde, G.; Baerends, E. J. *Theor. Chem. Acc.* **1998**, *99*, 391−403. te Velde, G.; Bickelhaupt, F. M.; Baerends, E. J.; Fonseca Guerra, C.; van Gisbergen, S. J. A.; Snijders, J. G.; Ziegler, T. *J. Comput. Chem.* **2001**, *22*, 931−967. Baerends, E. J.; Autschbach, J.; Bérces, A.; Bo, C.; Boerrigter, P. M.; Cavallo, L.; Chong, D. P.; Deng, L.; Dickson, R. M.; Ellis, D. E.; Fan, L.; Fischer, T. H.; Fonseca Guerra, C.; van Gisbergen, S. J. A.; Groeneveld, J. A.; Gritsenko, O. V.; Gruning, M.; Harris, F. E.; van den Hoek, P.; Jacobsen, H.; van Kessel, G.; Kootstra, F.; van Lenthe, E.; McCormack, D. A.; Osinga, V. P.; Patchkovskii, S.; Philipsen, P. H. T.; Post, D.; Pye, C. C.; Ravenek, W.; Ros, P.; Schipper, P. R. T.; Schreckenbach, G.; Snijders, J. G.; Sola, M.; Swart, M.; Swerhone, D.; te Velde, G.; Vernooijs, P.; Versluis, L.; Visser, O.; van Wezenbeek, E.; Wiesenekker, G.; Wolff, S. K.; Woo, T. K.; Ziegler, T. *Amsterdam Density Functional*, version 2004.01; S. C. M., Vrije Universiteit, Theoretical Chemistry: Amsterdam, The Netherlands, 2004.

(25) Perdew, J. P.; Burke, K.; Ernzerhof, M. *Phys. Rev. Lett.* **1997**, *78*, 1396.

(26) Versluis, L.; Ziegler, T. *J. Chem. Phys.* **1988**, *88*, 322−328.

(27) Mackay, S.; Gilmore, C. J.; Edwards, C.; Stewart, N.; Shankland, K. *maXus Computer Program for the Solution and Refinement of Crystal Structures*; Nonius, Delft, The Netherlands, MacScience, Japan, and University of Glasgow, Glasgow, Scotland, 1999.

(28) Altomare, A.; Cascarano, G.; Giacovazzo, C.; Guagliardi, A.; Burla, M. C.; Polidori, G.; Camalli, M. *J. Appl. Crystallogr.* **1994**, *27*, 435.

(29) Betteridge, P. W.; Caruthers, J. R.; Cooper, R. I.; Prout, K.; Watkin, D. J. *J. Appl. Crystallogr.* **2003**, *36*, 1487.

(30) Farrugia, L. J. *J. Appl. Crystallogr.* **1997**, *30*, 565.